Robust random telegraph conductivity noise in single crystals of the ferromagnetic insulating manganite $La_{0.86}Ca_{0.14}MnO_3$

J. Przybytek*
Institute of Experimental Physics, Faculty of Physics, University of Warsaw, 02-093 Warsaw, Poland

J. Fink-Finowicki and R. Puźniak
Institute of Physics, Polish Academy of Sciences, 02-668 Warsaw, Poland

A. Shames and V. Markovich
Department of Physics, Ben Gurion University of the Negev, 84105 Beer Sheva, Israel

D. Mogilyansky
The Ilse Katz Institute for Nanoscale Science and Technology, Ben-Gurion University of the Negev, 84105 Beer-Sheva, Israel

G. Jung
Institute of Physics, Polish Academy of Sciences, 02-668 Warsaw, Poland
and Department of Physics, Ben Gurion University of the Negev, 84105 Beer Sheva, Israel
(Received 9 August 2016; revised manuscript received 1 December 2016; published 1 March 2017)

Robust random telegraph conductivity fluctuations have been observed in $La_{0.86}Ca_{0.14}MnO_3$ manganite single crystals. At room temperatures, the spectra of conductivity fluctuations are featureless and follow a $1/f$ shape in the entire experimental frequency and bias range. Upon lowering the temperature, clear Lorentzian bias-dependent excess noise appears on the $1/f$ background and eventually dominates the spectral behavior. In the time domain, fully developed Lorentzian noise appears as pronounced two-level random telegraph noise with a thermally activated switching rate, which does not depend on bias current and applied magnetic field. The telegraph noise is very robust and persists in the exceptionally wide temperature range of more than 50 K. The amplitude of the telegraph noise decreases exponentially with increasing bias current in exactly the same manner as the sample resistance increases with the current, pointing out the dynamic current redistribution between percolation paths dominated by phase-separated clusters with different conductivity as a possible origin of two-level conductivity fluctuations.

DOI: 10.1103/PhysRevB.95.125101

I. INTRODUCTION

Electronic transport in mixed-valance manganites still lacks comprehensive theoretical explanations despite decades of intensive investigations. Experiments continue to reveal surprising facts, such as it is inconsistent with double-exchange ferromagnetic interactions' coexistence of insulating and metallic-like ferromagnetic phases in low-hole-doped $La_{1-x}Ca_xMnO_3$ (LCMO) manganites [1–5]. The ground state of LCMO at Ca-doping level $0.125 < x < 0.225$ is ferromagnetic and insulating (FMI). At higher hole-doping level $x > 0.225$ the ground state is ferromagnetic and metallic (FMM), while for $x < 0.125$ the ground state becomes insulating and antiferromagnetic [2]. The origin of the FMI state is still not clear. Several papers concluded that transport and magnetic properties of FMI phase are governed by superexchange and orbital ordering acting hand in hand with double exchange interactions [2,6]. Long-range interactions in the FMI phase may lead to freezing of charge carriers into electronic glass, opening of the Coulomb gap in the density of states, and hopping conduction in the presence of such a gap [4,7].

One of the characteristic features of mixed valance manganites is dynamic phase separation (PS), consisting in coexistence of phases with different orbital order and electronic properties. Phase separation stems from interplay of structural, charge, orbital, and spin degrees of freedom involving comparable energy scales. One of the consequences of such pronounced PS in low-doped manganites is the appearance of peculiar metastable states with different resistivities [6,8–10]. The metastable states are characterized by history-dependent conductivity, pronounced magnetization and resistivity relaxation, resistance memory effects, and strong low-frequency conductivity noise. The conductivity noise is typically of $1/f$ type but at low temperatures may exhibit peculiar non-Gaussian or nonequilibrium character [4,11,12]. The non-Gaussian components of the noise frequently take the form of random telegraph noise (RTN), consisting in random jumps of the conductivity between two fixed levels, referred to as *up* and *down* states, while the lifetimes of each of the two levels are exponentially distributed. Generation of RTN noise can be generally traced to an action of a two-level fluctuator (TLF) consisting of two energy wells separated by a barrier.

In general, telegraph noise can be observed when the size of the system is reduced to such an extent that it contains only a few or just one single active two-level fluctuator. In larger samples, the non-Gaussianity of the noise is a signature of a single, or just a handful, of elementary fluctuators influencing system properties on a length scale comparable with the system size. In strongly inhomogeneous and phase separated bulk

*jacek.przybytek@fuw.edu.pl

materials with percolation-like conductivity, even above the percolation threshold there will be always local bottlenecks in the conducting paths which funnel the current and lead to large local voltage drops. Active fluctuators located in the vicinity of such bottlenecks can give rise to RTN fluctuations also in macroscopic samples.

Random telegraph noise in colossal magnetoresistive (CMR) manganites is ascribed to two possible mechanisms. On one hand, it is regarded as a spectacular manifestation of PS and coexistence of percolating paths with significantly different conductivity [13–19]. On the other hand, it is ascribed to strong fluctuations of magnetic moments, most prone to occur in the vicinity of the paramagnetic (PM) to ferromagnetic (FM) phase transition, which couple to the resistivity through a pronounced CMR effect [14,15]. Two-level resistance switching with amplitudes ranging from 0.01 to 0.2% has been reported in $La_{1-x}Ca_xMnO_3$ (LCMO) crystals and thin films [14–17]. Multilevel RTN with amplitudes in the range of 10% of the total sample resistance has been found in highly resistive $Pr_{1-x}Ca_xMnO_3$ system, characterized by current induced switching into metastable high-resistivity states [13,18]. We have reported bias-sensitive giant RTN with amplitude exceeding 10% of the total sample resistance in LCMO doped at $x = 0.18$ [20]. RTN fluctuations were also associated with electronic phase transitions in manganites at low temperatures [21,22].

Recently, we have reported on the peculiar metastable behavior of freshly grown $La_{0.86}Ca_{0.14}MnO_3$ single crystals, which under continuous thermal cycling between room temperature and liquid helium, accompanied by multiple dc bias current cycles, spontaneously evolved towards the lower resistivity state [23]. The situation is quite similar to that observed by us previously in LCMO crystals with Ca doping closer to the percolation threshold, $x = 0.18$, 0.20, and 0.22 [8–10]. However, in a difference to our previous experiments, we were not able to influence in a controlled way the development of metastable states in $La_{0.86}Ca_{0.14}MnO_3$ by means of electric current and field procedures.

A transition to the low-resistivity metastable state is reflected in the noise characteristics of the investigated crystals. While the conductivity noise in the pristine high-resistivity state is almost exclusively of $1/f$-like character, the noise in the low-resistivity state shows pure $1/f$-like spectra only at room temperatures. Moreover, the level of the normalized $1/f$ noise in the low-resistivity state is higher than the level of the noise in the high-resistivity state [23]. Most importantly, however, with decreasing temperature an additional excess noise component appears in the low-resistivity metastable state and eventually dominates the entire spectral behavior. The excess noise appears as a Lorentzian-like spectral component, which in time domain takes form of a clear two-level random telegraph noise, as shown in Fig. 1. It follows from Fig. 1 that the duty cycle of the noise is asymmetric with respect to the bias current polarity, indicating that resistivity fluctuations are the source of the observed telegraph voltage fluctuations. The observed amplitude of RTN signal, i.e., the difference between resistances in the *up* and *down* RTN states, was of the order of 10^{-3} of the total sample resistance.

Several features of RTN conductivity fluctuations observed in the low-resistivity metastable state are quite unusual. First

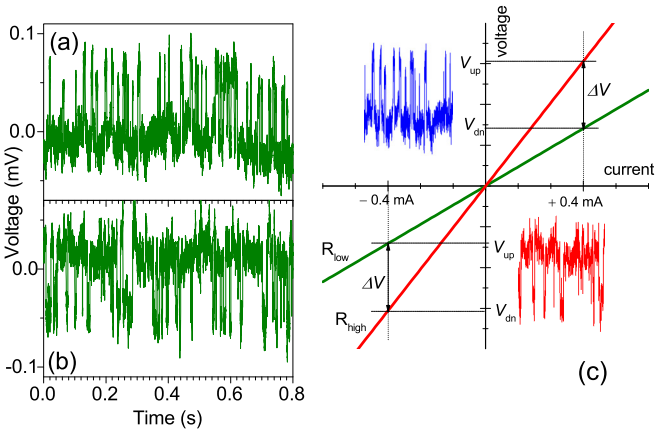

FIG. 1. RTN time traces at $T = 160$ K for two equal dc bias currents with opposite polarizations: (a) positive current $I = 0.4$ mA and (b) negative current $I = -0.4$ mA. (c) Schematics of $I - V$ characteristics of high- and low-resistivity states and RTN switching between them with amplitude $\Delta V = V_{up} - V_{dn}$ showing the inversion of RTN duty cycle upon changing the polarity of the bias current.

of all, the responsible two-level fluctuator has a macroscopic character and affects the resistance of the entire bulk sample. Moreover, RTN onsets in the paramagnetic state, around 185 K, well above the Curie temperature $T_c = 167$ K determined from the magnetization measurements, and persists in exceptionally wide temperature range of about 50 K, down to 130 K. The switching rates of the RTN are clearly thermally activated, but within the experimental accuracy, they are completely independent of bias current and magnetic field. The voltage amplitude of the RTN noise is also temperature dependent but, surprisingly, decreases with increasing bias current, pointing out to a nontrivial mechanism in which the difference between resistivity of the high and low RTN states decreases with increasing bias current stronger than in the linear way. The observed RTN noise is quite reproducible. It reappeared in several subsequent thermal cycles and showed similar characteristics, provided the sample endured in the low-resistivity state.

In order to understand the mechanism of such robust RTN conductivity fluctuations we have performed comprehensive characterization of $La_{0.86}Ca_{0.14}MnO_3$ crystals by means of noise, structural, magnetic, transport, and electron magnetic resonance (EMR), comprising electron paramagnetic resonance (EPR) and ferromagnetic resonance (FMR) measurements. One of the key questions is the nature of the *up* and *down* RTN resistance levels which are most likely associated with coexistence of clusters of phases with different electronic and magnetic properties. Magnetic resonance technique is known to provide an insight into the nature and temperature evolution of phase-separated magnetic and electronic states in doped manganites [24,25].

II. EXPERIMENTAL

We have grown single crystals of $La_{0.86}Ca_{0.14}MnO_3$ from sintered ceramic rods of high-purity commercial La_2O_3, $CaCO_3$, and MnO_2 precursors by means of the floating zone technique. To account for smaller than one Ca segregation

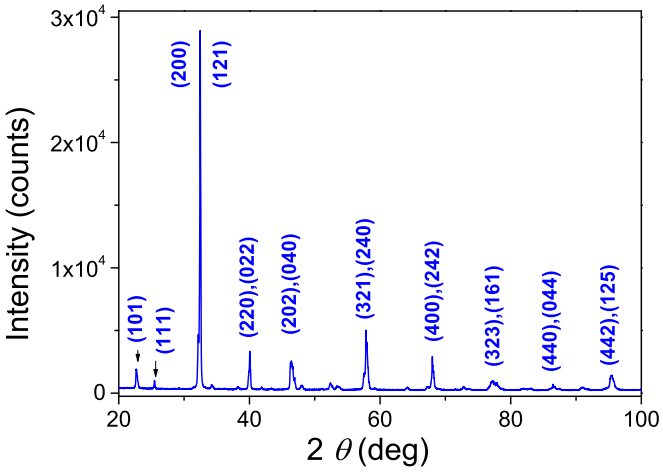

FIG. 2. XRD spectra of $La_{0.86}Ca_{0.14}MnO_3$ crystal, indexed in the orthorhombic setting of the *Pnma* space group.

coefficient and to compensate for the evaporation of manganese during the crystallization process, the starting rods were prepared with slight excess of Ca and Mn content. The crystals were grown in air, using a double-mirror 2.5-kW high-pressure xenon lamp optical furnace. The speed of growth was 2.5 mm/h and a previously grown single crystal was used as a seed. During the growth process the feed rod and the seed crystal were rotated in opposite directions with the rate of 10–20 rpm.

The quantitative analysis of the chemical composition was performed on the polished planes of the crystals by field emission scanning electron microscopy. The average chemical composition was checked by scanning electron microscopy and EDX analysis. Phase analysis of the crystals was performed at room temperature by x-ray powder diffraction. The diffraction peaks were indexed in the orthorhombic setting of the *Pnma* space group and the Rietveld analysis of XRD spectrum, see Fig. 2, was employed to refine the lattice parameters. The lattice parameters were found to be $a = 5.550(2)$ Å, $b = 7.761(4)$ Å, and $c = 5.512(2)$ Å, and the unit cell volume $V = 237.5$ Å^3, thus independently verifying the doping level of $x \approx 0.14$ [2].

As grown crystals consisted of large randomly oriented blocks. The dominant orientation within the blocks was determined using a four-circle x-ray diffractometer. Samples for transport and noise measurements were cut off from the areas with well-defined orientation. Individual samples had form of 1-mm-thick and 3-mm-wide bars directed along the [100] crystalline direction. Current and voltage leads were indium soldered to the vacuum evaporated gold contacts. Transport and noise characteristics were measured in a standard four-point contact arrangement with 0.33 mm distance between the voltage contacts. Voltages developing across current-biased sample were amplified by very-low-noise room-temperature preamplifier located on the top of the cryostat and processed by a computer. Because of relatively high impedance of the samples, especially at low temperatures, particular attention was paid to the level of the signal at the amplifier input to avoid the saturation and not to exceed the allowed common voltage level during data acquisition. Noise characteristics were measured in function of temperature and bias, both in cooling and heating regime, by stabilizing the temperature at the required set point and acquiring spectra and time domain voltage traces for different values of dc current bias. In the frequency domain, the instrumental noise originating from the measuring chain and contacts was eliminated by subtracting the reference spectrum, recorded at each temperature with zero current flow in the sample, from the spectrum acquired with the current bias.

Measurements of static resistivity $R = V/I$ were performed under dc current bias, in parallel with the noise measurements, by dc coupling the voltage signal and maintaining the same bias and temperature settings.

The ac susceptibility and dc magnetization measurements were carried out with Quantum Design Magnetic Property Measurement System (MPMS XL) equipped with ac-susceptibility option. The temperature dependence of the magnetization was measured by cooling the sample down to $T = 10$ K in zero magnetic field, applying a constant magnetic field at low temperature, and measuring the zero-field-cooled (ZFC) magnetization upon heating to 300 K. Zero-field-cooled run was followed by measurements of the field-cooled (FC) magnetization in a subsequent cooling run in a constant magnetic field. The temperature dependence of ac susceptibility was measured at several frequencies between 1 Hz and 1 kHz, with the probing field amplitude of 1 Oe in warming mode.

Electron magnetic resonance (EMR) measurements were performed with Bruker EMX-220 x-band spectrometer operating at 9.466 GHz with 50 μW of incident microwave power. The magnetic field was modulated at 100 kHz with the amplitude of 3 Oe. For EMR measurements we have employed a few milligrams of fine powdered crystal. The loose-packed form of the fine powdered sample enables one to exclude the influence of the skin effect and to narrow the signals in the FM state due to the texture of fine particles in the external magnetic field [26]. This, in turn, offers an opportunity to examine complex EMR signals in more detail. In the course of the experiments, we have analyzed the temperature dependences of the resonance field H_r, peak-to-peak line width H_{pp}, and the doubly integrated intensity (DIN), which is proportional to the EMR susceptibility χ_{EMR}.

III. RESULTS

A. Transport properties

Temperature and bias-current dependence of the resistance of $La_{0.86}Ca_{0.14}MnO_3$ crystal is shown in Fig. 3. For this LCMO crystal we were not able to fully control the development of metastable resistivity states by means of electric current/field procedures, in a marked difference to LCMO crystals Ca-doped closer to but still below the percolation threshold, $x = 0.18$, 0.20, and 0.22, previously investigated by us [8–10]. In the first few days of the experiments, the temperature dependences of the resistivity of the freshly crystallized sample clustered into a high resistivity state, labeled as HRS in the Fig. 3. During the consecutive thermal cycling between room temperatures and liquid helium temperatures, accompanied by application of multiple dc bias current cycles, the resistivity of

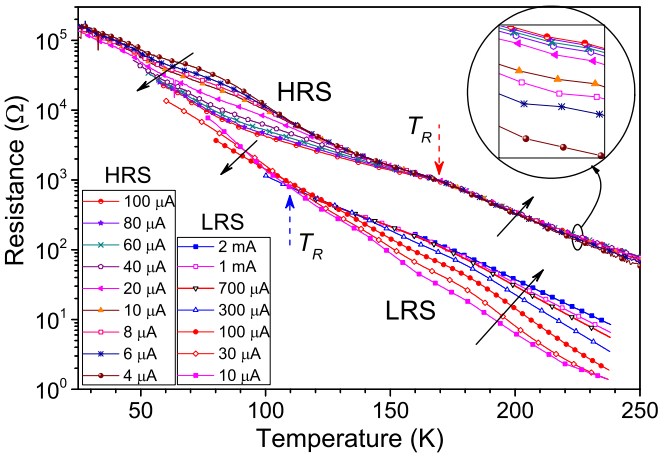

FIG. 3. Temperature and bias-current dependence of the resistivity of $La_{0.86}Ca_{0.14}MnO_3$ in the pristine HRS and in the metastable LRS. Dashed arrows indicate the temperatures T_R at which sample resistivity becomes locally bias independent. Solid arrows across the data indicate the direction of current increase. The subsequent increasing current values are listed in the tables shown in the lower left inset to the figure for HRS and LRS, respectively.

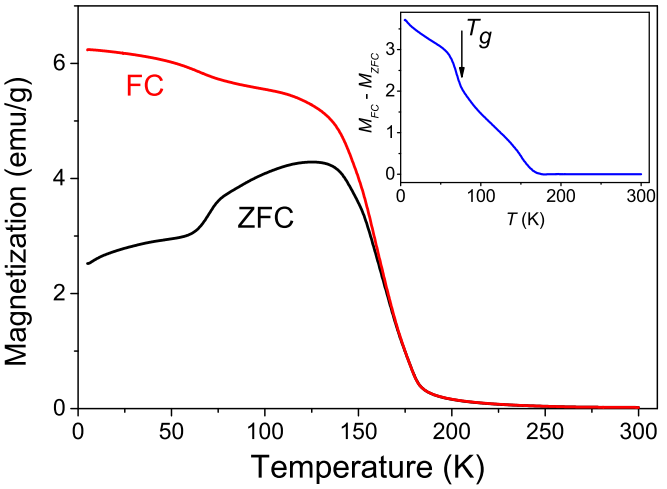

FIG. 4. Zero-field-cooled (ZFC) and field-cooled (FC) dc magnetization measured at 100 Oe for $La_{0.86}Ca_{0.14}MnO_3$. Inset shows the difference between FC and ZFC magnetization as a function of temperature.

the studied $La_{0.86}Ca_{0.14}MnO_3$ crystal spontaneously evolved towards the low-resistivity metastable state, labeled LRS in Fig. 3. Samples remained in this state for the next two months, despite continuous experimentation involving thermal and bias cycling. However, after a three-month-long break in the experiments, during which the LCMO crystal was stored at room temperatures, the sample spontaneously returned to the pristine high-resistivity state and persisted in this state during the next two months of continuous experimentations.

Figure 3 shows that both above and below Curie temperature T_c, the resistance of pristine HRS and metastable LRS strongly increases with decreasing temperature in a thermally activated way. Although the resistivity depends on the bias current, the effect being most prominent in the LRS at higher temperatures, the overall activated character of $R(T)$ curves in both states is essentially identical and does not depend on the level of bias current or direction of the temperature change. Observe that at high temperatures, both LRS and HRS resistivities increase with increasing current, while at low temperatures they decrease with increasing current. For both HRS and LRS there exists a temperature T_R (see Fig. 3) at which all the $R(T)$ curves cross and the direction of the resistivity variation with increasing current inverts. For pristine HRS the temperature T_R is close to T_c, while in the LRS the value of $T_R \approx 110$ K. At temperatures below respective T_R, HRS and LRS resistivities decrease with increasing bias.

Temperature dependence of the resistivity of LCMO crystals doped closer to the percolation threshold always exhibit a pronounced maximum associated with the metal-to-insulator (M-I) transition in the vicinity of T_c [8–10]. The $R(T)$ dependence of $La_{0.86}Ca_{0.14}MnO_3$ shows only a slight change of the slope at $T \approx T_c$. Monotonously increasing resistivity with decreasing temperature evidences relative weakness of the ferromagnetic metallic state in the $La_{0.86}Ca_{0.14}MnO_3$ system and effective domination of the ferromagnetic insulating state at temperatures below T_c.

B. Magnetic properties

Temperature dependence of the field-cooled M_{FC} and zero-field-cooled magnetization M_{ZFC} of $La_{0.86}Ca_{0.14}MnO_3$ sample is shown in Fig. 4. The curves were recorded at applied field of 100 Oe. The $M_{ZFC}(T)$ and $M_{FC}(T)$ curves diverge at the irreversibility temperature $T_{irr} \approx 160$ K, see inset in Fig. 4, and the difference between them increases strongly with decreasing temperature. At low temperatures M_{ZFC} slightly decreases with decreasing temperature. The Mn spin sublattice undergoes relatively broad magnetic transition at Curie temperature $T_c = 167 \pm 0.5$ K, as determined from the temperature of a minimum in the derivative $dM_{FC}(T)/dT$. Below the temperature $T_g \approx 80$ K, at which M_{ZFC} and $M_{FC}(T)$ change slope, the splitting between zero ZFC and FC curves significantly increases.

The temperature dependence of the real χ' and imaginary part of ac susceptibility χ'' is shown in Figs. 5(a) and 5(b). The real part of ac susceptibility shows a peak at $T_p \approx 154$ K and significant frequency dependence in a wide temperature range between 75 K and T_p. Within this temperature range, χ' decreases with increasing frequency but becomes practically frequency independent below $T \approx 60$ K. Moreover, at $T \approx 80$ K, $\chi'(T)$ changes slope in a manner similar to that of other low-doped LCMO crystals [9]. The imaginary part of ac susceptibility demonstrates two peaks. The first one, appearing at $T \approx 160$ K, may be associated with the PM to FM transition, while the low-temperature peak is related to freezing of magnetic moments at $T = T_g$. The position of T_g shifts to higher temperatures with increasing frequency, a typical behavior of spin glasses. The effect is quite significant: T_g changes by 11 K within the frequency interval of 10 Hz to 10 kHz, resembling closely the previously observed behavior of other low-doped LCMO single crystals [9]. In spin/cluster glasses, the shift of the freezing temperature under the frequency change of $\Delta\omega$ is usually characterized by the factor $K = \Delta T_g/[T_g \Delta(\log \omega)]$ [27]. The K factor for $La_{0.86}Ca_{0.14}MnO_3$ crystal is $K \approx 0.05$, and falls into the range

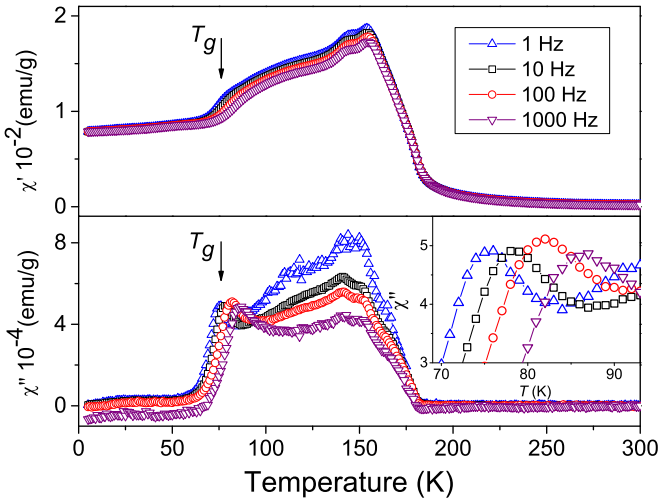

FIG. 5. Temperature dependence of real and imaginary components of ac susceptibility, measured during warming, at the probing ac field with different frequencies and amplitude $H_{ac} = 1$ Oe. Arrows indicate the position of the frequency-dependent freezing temperature T_g. The frequency dependence of T_g is clearly visible in the zoom of $\chi''(T)$ shown in the inset.

typical for spin-glass values. It is well known that in canonical spin-glasses ZFC and FC magnetization start to differ only very close to the spin-glass freezing temperature T_g [27]. In a marked difference, the irreversibility temperature of the studied LCMO crystal is significantly higher than the freezing temperature, a feature pointing out to a possible cluster-glass behavior; see Ref. [28] and references therein.

C. EMR properties

Temperature evolution of $La_{0.86}Ca_{0.14}MnO_3$ EMR spectra is illustrated in Fig. 6. At room temperature, the EMR spectrum shows a symmetric Lorentzian-like singlet line with peak-to-peak line width $H_{pp} = 720$ Oe and the g factor equals 1.99 ± 0.01, typical for perovskite manganites in the paramagnetic regime [29]. Upon decreasing temperature, the singlet line converges and slightly shifts towards lower fields. The signal retains its Lorentzian shape down to $T \approx 190$ K, but around $T = 240$ K an additional spectral component, marked with a dashed arrow in Fig. 6(b), appears on the low-field shoulder of the main line. The additional component, referred to as FM1, may be associated with the ferromagnetic phase with Curie temperature higher than T_c of the main FM phase, referred to as FM2. The intensity of the FM1 line grows with decreasing temperature, while its resonance position slightly shifts towards lower fields. We associate the FM1 line with the ferromagnetic metallic phase FMM, because its behavior resembles very closely that of the main FM metallic phase in LCMO doped at $x = 0.19$, reported in detail in Ref. [25].

At 185 K the main Lorentzian-like FM2 line starts to be asymmetric and splits into two lines: low-field FM2-LF, and high-field FM2-HF, line. Below 150 K, FM2-LF line broadens and shifts toward zero field, while FM2-HF line also broadens but shifts towards higher fields. The most intensive FM2 signal may be attributed to strongly anisotropic FM insulating phase FMI [25]. It follows from the behavior of

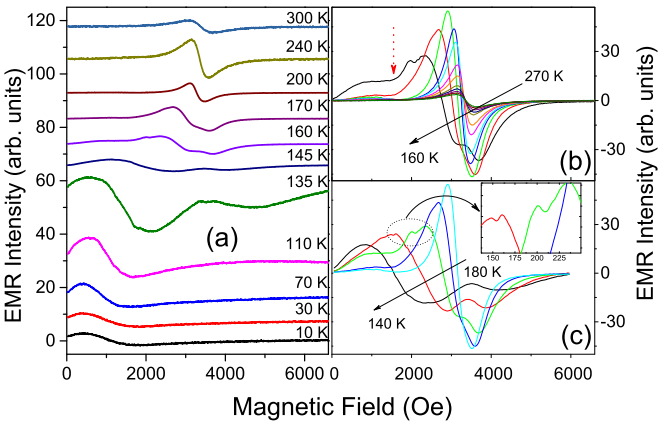

FIG. 6. (a) Temperature evolution of EMR spectra. The recordings are shifted vertically for clarity. The intensity of lines in the range 145–200 K is reduced by a factor of 10 to fit them into the graph. (b) Zoom into the temperature evolution between 270 and 160 K. The red dashed arrow points out the contribution attributed to FM1 component. (c) Evolution of EMR spectra across the PM to FM transition, in the range 140 K $< T <$ 180 K. Inset shows the spectra appearing just below T_c with appearance of additional small sharp lines. Arrows in panels (b) and (c) indicate the direction in which the temperature is decreasing in 10-K steps.

the EMR peak-to-peak line width H_{pp} and resonance field H_r, shown in Fig. 7, that below 150 K, FM1 and FM2-LF signals are practically indistinguishable within a certain temperature range. At $T = 130$ K, the FM2-LF line becomes unobservable. The FM2-HF line is still observable down to 105 K, when it moves out of the spectrometer magnetic field range. At temperatures below 100 K, only the FM1 line remains in the EMR spectrum. At temperatures just below T_c, additional sharp lines, with the width of the order of 60 to 100 Oe, appear on the top of the main FM2 line, as illustrated in the inset to Fig. 6(c). One may attribute these lines to FM domains whose magnetic field driven growth is temporarily terminated or hindered by pinning of the edges of FM clusters by lattice defects or crystallite structure boundaries [30]. The volume of hindered FM domains, estimated from the intensity of the corresponding lines, constitutes 10^{-6}–10^{-5} of the total volume of the FM2 phase. When applied magnetic field H becomes

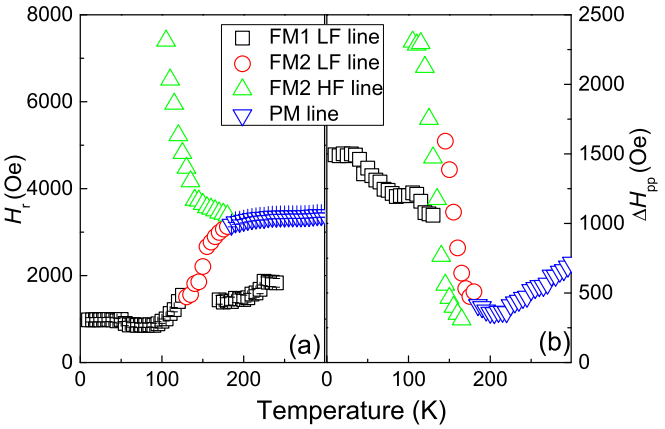

FIG. 7. Temperature dependence of EMR peak-to-peak line width H_{pp} and resonance field H_r.

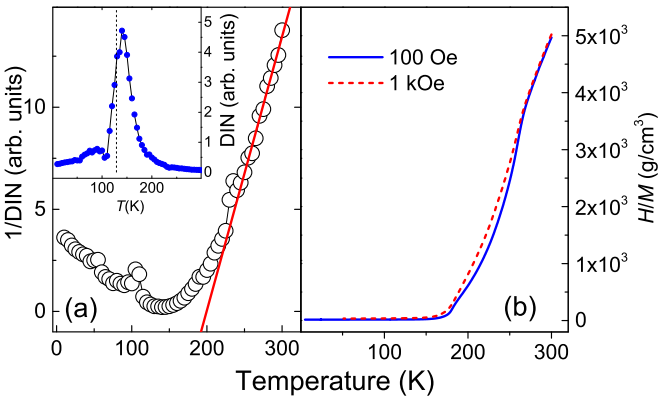

FIG. 8. (a) Inverse EMR double integrated intensity (DIN). Solid line is drawn according to the best fit of the Curie-Weiss law to the data. Inset shows temperature dependence of DIN. The dashed line marks the temperature at which the low field signal of FM2 becomes unobservable. (b) Temperature evolution of the inverse dc magnetic susceptibility.

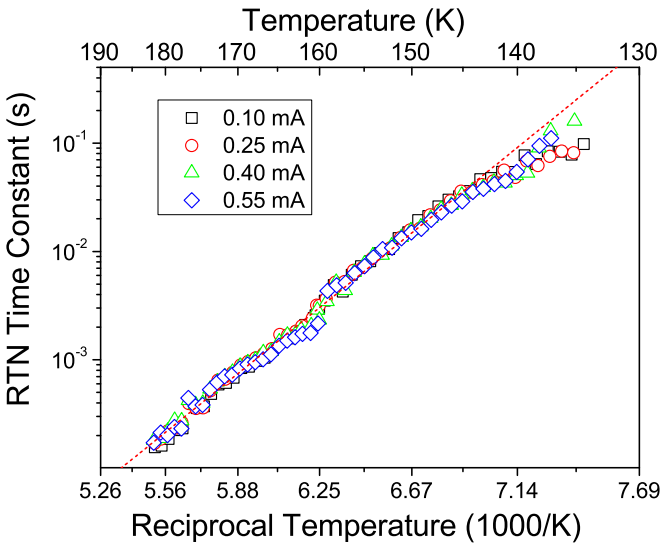

FIG. 9. Evolution of RTN time constant with temperature for different bias currents.

strong enough to overcome the pinning energy, the pinned clusters disappear and merge into the growing volume of the FM2 phase.

Doubly integrated intensity (DIN) of the entire EMR signal is shown in the inset to Fig. 8(a). The intensity increases with decreasing temperature, reaches the maximum at $T = 140$ K, and drops down with further temperature decrease. A strong decrease of the DIN is observed down to 100 K. At that temperature both FM2 components become unobservable due to strong broadening and shifting out of the magnetic field limits. Below 100 K, the intensity and the width of the remaining FM1 line change slowly with temperature, decreasing down to $T = 10$ K, as shown in Fig. 7.

Temperature dependence of inverse DIN, which is proportional to the EMR susceptibility χ_{EMR}, along with the temperature dependence of the inverse dc susceptibility $\chi_{dc} = H/M$, are illustrated in Fig. 8. Significant field-dependent deviations from the Curie-Weiss (C-W) law are clearly visible in the figure. Such features are observed in many manganite systems and are frequently interpreted as manifestations of the Griffiths phases [31]. In an alternative approach, these features are seen as signatures of the inhomogeneity and magnetic disorder in the sample [32]. In our case, the deviations from the C-W law are related to the appearance of the FM1 phase at temperatures above the Curie temperature.

Our EMR results are generally consistent with literature reports on similarly doped LCMO with $x = 0.125$ and $x = 0.15$ [25]. Nevertheless, there are also significant differences between our results and the literature data. For both $x = 0.125$ and $x = 0.15$, minor contributions from ferromagnetic inhomogeneities, characterized by weaker magnetic anisotropy, were revealed at low temperatures. Formation of spatially separated ferromagnetic regions in the paramagnetic regime was observed only in LCMO samples with x above 0.175 [25]. In the studied crystals, the additional FM1 phase appears at temperatures much above the FM transition temperature for the main FMI phase FM2, and the presence of this phase is responsible for unusual magnetic, transport, and noise properties within the range $T_c < T < 240$ K.

D. Random telegraph conductivity noise

Temperature and bias dependences of the characteristic time constant of the RTN fluctuations $\tau = \tau_{up}\tau_{dn}/(\tau_{up} + \tau_{dn})$, where τ_{up} and τ_{dn} are the average lifetimes in the *up* and *down* RTN states, respectively, are illustrated in Fig. 9. The time constant was determined by fitting to the experimental spectra the sum of A/ω^{α}, $1/f$-like contribution of intensity A and spectral slope α, and Lorentzian term S_L with the characteristic switching rate τ and jump amplitude ΔV,

$$S_V(\omega) = S_{1/f} + S_L = \frac{A}{\omega^{\alpha}} + 4\Delta V^2 \frac{r}{(1+r)}\frac{\tau}{(1+\omega^2\tau^2)}, \quad (1)$$

where $r = \tau_{up}/\tau_{dn}$ accounts for the asymmetry in the RTN signal and can be expressed in terms of the duty cycle $D = \tau_{up}/(\tau_{up} + \tau_{dn})$ as $r = D/(1-D)$. The procedure was verified by comparing RTN amplitudes determined from the above spectral fit with the difference between centers of two Gaussian obtained by fitting the histogram of the signal in the time domain to the sum of two Gaussian distributions. The agreement between the fitting procedures was excellent.

It follows from Fig. 9 that the RTN process is thermally activated. The activation energy obtained by fitting the Arrhenius law to the temperature dependence of the RTN effective rate—the best fit is shown by a dotted line in Fig. 9—was found to be $E_a = 300 \pm 0.3$ meV with the prefactor $\tau_0 = (1 \pm 0.28) \times 10^{-12}$ s, falling into the expected range of phonon frequencies in solid state. However, as shown in Fig. 9, the switching rate is practically completely bias current/voltage independent.

The same concerns the duty cycle of the RTN wave form D, which changes with temperature but remains insensitive to the bias current and voltage, as illustrated in Fig. 10. At high temperatures the RTN signal spends most of the time in the *down* state, similar to the RTN described by Raquet *et al.* [16]. With decreasing temperature, the RTN waveform becomes more symmetric and D increases and

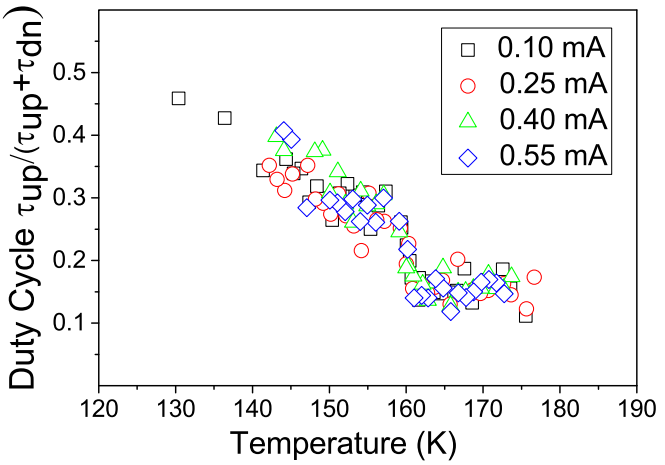

FIG. 10. RTN duty cycle dependence on temperature for different currents.

eventually almost reaches a symmetric value $D = 0.5$ at the temperature at which the amplitude of RTN vanishes.

At each temperature, the amplitude of the robust RTN is strongly decreasing with increasing current bias, as shown in Fig. 11. The temperature dependence of the amplitude is, however, nonmonotonous. With decreasing temperature, the amplitude increases at temperatures above T_c, then goes through a maximum, followed by a decrease to zero with further temperature decrease. The RTN signal disappears below $T = 130$ K, namely due to the vanishing amplitude.

IV. DISCUSSION

Let us first provide convincing evidence that the observed telegraph noise is not an artifact resulting simply from extrinsic effect of contacts, and in particular from noise injected by current contacts or from shunting of the current in highly resistive crystal by metallic pads of voltage measuring contacts. Shunting effects may become significant, especially for contacts separated by distances comparable to or smaller than the sample thickness, as in our case. To verify that contact effects are not disturbing our measurements, we have initially checked that the noise volume does not depend on the sample volume by using different sets of voltage contacts, separated by 1.6 and 0.33 mm. The noise volume measured at $T = 200$ K was 2.5×10^{-19} m^3 and 2.8×10^{-19} m^3, respectively. These tests allowed us to conclude that excess contact/interface noise or and shunting effects do not contribute to the measured noise [33]. Moreover, different behavior of the high- and low-resistance states provides the straightforward argument that the observed RTN is not an artifact due to contact effects. In the same sample with the same contact arrangement, RTN appears only in the low-resistivity state and is absent in the high-resistivity state, while contact shunting effects should be in fact more pronounced in the high-resistance state.

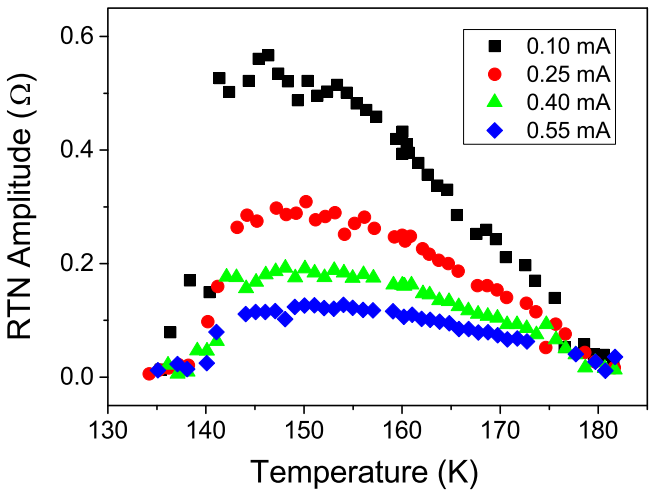

FIG. 11. Evolution of RTN amplitude with temperature for different bias currents.

As pointed out in the introduction, there are two most plausible mechanisms behind RTN conductivity noise in mixed valance manganites, PS resulting in dynamic coexistence of clusters with different conductivities or magnetic moment fluctuations coupling to the resistivity through the CMR effect. The temperature range in which the robust RTN is observed coincides exactly with the temperature range of the broad FM transition of our sample; compare Figs. 11 and 4. Moreover, RTN amplitude reaches its maximum at the same temperature at which the imaginary part of ac susceptibility goes through the maximum. These facts strongly suggest possible magnetic origin of the observed RTN. However, the RTN switching rate is practically not affected either by the bias current or by the applied magnetic field.

The maximal magnetic field that we could apply in our noise experiments was limited to some 100 Oe. Nevertheless, literature reports concerning magnetic moment fluctuations as a source of RTN fluctuations in mixed valance manganites show that fields much lower than 100 Oe already cause significant changes in RTN switching rate and duty cycle [15]. Therefore, one may reject magnetic fluctuations as a possible mechanism behind the observed RTN. Moreover, our data show no specific noise features in the vicinity of temperature T_g at which, as revealed by the magnetic measurements, the spin system in the studied crystals freezes into the glassy state. If the magnetic degree of freedom is involved in the fluctuation mechanism one expects to see a noise maximum around the freezing temperature T_g [34].

The above considerations direct us to look for the phase-separation-based mechanism in which current flow through inhomogeneous PS sample has a percolating character. Percolating current may switch between percolation paths constituted by clusters dominated by phases with different resistivity. We have to exclude mechanisms related to electronic charge ordering phase separation, like those found to be responsible for telegraph conductivity fluctuations in the nonlinear $I - V$ regime in $Pr_{0.63}Ca_{0.37}MnO_3$ single crystals [21], because our RTN signal persists in a much wider temperature range. Moreover, for a low-doped LCMO system, no charge ordering but only orbital ordering has been discovered. The ordering temperature is almost independent of Ca-doping level and falls below 100 K, well below the temperature range in which we have observed our robust two-level fluctuations [2].

Our EMR and magnetization measurements clearly show that below 240 K metallic-like FM1 phase coexists with

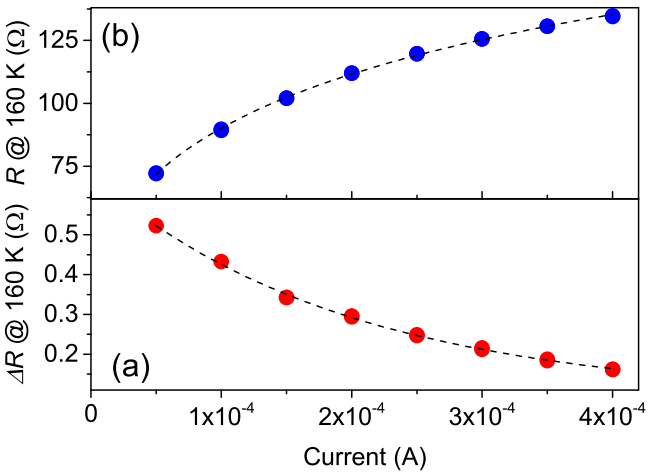

FIG. 12. (a) RTN amplitude ΔR at 160 K as a function of bias current I. (b) Sample resistance R at 160 K as a function of bias current I. The dashed lines are the best fits of the exponential function $a + b\exp(-kI)$ to the data.

high-resistivity PM phase. FM1 clusters are only short range correlated and cannot form long low-resistivity percolation paths. Long-range FM correlations onset at 185 K together with the appearance of the major insulating FM2 phase. Therefore, down to 185 K, the sample persists in the superparamagnetic (SPM) state. Long-range correlations enable formation of long percolation paths, dominated by a cluster of FM phases with different resistivities. Within the entire temperature range of SPM-to-FM transition the role of different resistivity phases is played by coexisting insulating FM2 and metallic FM1 ferromagnetic phases. Analysis of the temperature dependence of DIN enables one to estimate that at low temperatures, the FM1 phase constitutes about 10% of the total FM phase volume.

In the search for responsible physical mechanism one has to note that at a fixed temperature, RTN amplitude strongly decays with increasing bias current. In the same time, the sample resistance strongly increases with increasing current, so remember that the sample stays in the low-resistivity metastable state. The form of the RTN amplitude dependence on current seen at 160 K and bias current dependence of the sample resistance at the same temperature are confronted in Figs. 12(a) and 12(b). The temperature of 160 K is close to the one at which RTN amplitude is maximal, what enables the most accurate RTN amplitude measurements in a wide bias range.

It follows that both RTN amplitude decay and sample resistivity increase with increasing current are best fitted by the exponential function $y = a + b\exp(-kI)$. The function fits the amplitude dependence with $a = (0.09 \pm 0.5)\,\Omega$, $b = (0.556 \pm 0.007)\,\Omega$, and $k = (5100 \pm 240)\,\mathrm{A}^{-1}$, while the resistivity fit converges with parameters $a = (147 \pm 0.5)\,\Omega$, $b = (-96 \pm 0.4)\,\Omega$, and $k = (5020 \pm 80)\,\mathrm{A}^{-1}$.

Observe that the best fit to both RTN amplitude and resistivity bias dependence is obtained with the same value of exponent k, strongly suggesting that the same physical mechanism is responsible for variations of RTN amplitude and sample resistance with bias current. This enables us to suggest a toy model of RTN conductivity fluctuations in which RTN results from switching of a fraction β of the total sample resistance between current-dependent low resistivity $R(T,I)$ and current-independent saturated high resistivity $R_h(T)$. Within such a scenario the RTN amplitude becomes

$$\Delta R(I,T) = \beta[R_h(T) - R(I,T)], \tag{2}$$

and specifically at $T = 160$ K, by using parameters obtained in fitting procedures, one gets

$$\begin{aligned}\Delta R(I,160K) &= (0.09 + 0.556e^{-kI})\Omega \\ &= \beta[R_h(160\ \mathrm{K}) - 147 + 96e^{-kI}]\Omega. \end{aligned}\tag{3}$$

Assuming that within an experimental error, the exponential factors k in the functions fitting $R(I,160\ \mathrm{K})$ and $\Delta R(I,160\ \mathrm{K})$ are equal, one obtains that $R_h(160\ \mathrm{K}) = 163\ \Omega$ and $\beta = 5.7 \times 10^{-3}$. Observe that thus obtained value of the saturated resistance $R_h(160\ \mathrm{K})$ corresponds exactly to the value of resistance measured directly in the experiment at high currents, see Fig. 3, which proves the consistency of the proposed toy model.

If the current flow in the sample would be homogenous, the estimation of the parameter β would enable an evaluation of the volume of the sample taking part in the RTN switching process as $V_{\mathrm{TLF}} = \beta V_s = 5.9 \times 10^{-12}\ \mathrm{m}^3$, where $V_s = 9.9 \times 10^{-10}\ \mathrm{m}^3$ is the volume of the sample contained between the voltage contacts. Obviously, due to the percolating nature of the current flow, it is not homogenous and the above estimation gives us only an upper limit of the active volume of the sample participating in the RTN generation.

On the basis of the above observations we propose that RTN switching occurs between the saturated resistance of the percolation path, current independent resistance seen at high levels of the current flow and some lower, current-dependent resistance. We suggest that dynamic current redistribution mechanism [35] is responsible for switching between such determined RTN levels. To illustrate the proposed mechanism, let us assume that an active two-level fluctuator is initially in the *up* state, meaning that the current is percolating through the sample along a path with a high, saturated resistance. Whenever a lower resistance path will be available in the close vicinity to the saturated path, the current distribution would change and switch, by means of thermal activation, to the lower resistivity network. This results in a transition of the RTN signal from *up* to the *down* level. However, simultaneous decrease of the current in the saturated resistivity percolation path decreases its resistance and turns it into a low-resistance path capable of shunting the current from the environment. Current distribution changes again in a thermally activated way and moves to the new path. This appears as transition back to the *up* RTN state since the current flows along the previous percolation path with saturated higher resistance.

The very dynamic current redistribution mechanism can be responsible for the vanishing of RTN amplitude at low temperatures because the driving force behind RTN switching, current dependence of the resistance, monotonously diminishes with decreasing temperature; see Fig. 3. The RTN amplitude $\Delta R(I,T)$ disappears and becomes zero when sample resistivity stops depending on the current

flow and $R_h(T) - R(I,T) = 0$, which in the low-resistivity state happens around 120 K. The RTN amplitude, however, initially increases with decreasing temperature, despite diminishing of the bias influence on resistivity. This is due to simultaneously increasing volume of low-resistivity phase FM1 with decreasing temperature, as revealed by our magnetic resonance measurements. The volume of the ferromagnetic phase stabilizes below the SPM-FM transition and the RTN amplitude decreases with further temperature decrease due to the diminishing effect of the bias current. The maximum of the RTN amplitude is observed at the crossover temperature of both effects, namely just below T_c.

We have observed significant RTN fluctuations only in the sample persisting in the low-resistivity metastable state. When after few months the sample spontaneously returned to the high-resistivity state, the RTN fluctuations disappeared. Nevertheless, as will be discussed in detail elsewhere, through the measurements of the second spectra [34] of the conductivity noise we have determined that at temperatures at which RTN in LRS reaches its maximum, the non-Gaussian component of the HRS $1/f$ conductivity noise also goes through a strong local maximum. Further increase of the non-Gaussian noise in HRS is observed again at lower temperatures where the resistivity starts to be pronouncedly dependent on the current flow. In this temperature range we were able to detect clear thermally activated Lorentzian features in the conductivity noise spectra but were not able to resolve clear RTN wave forms in the time domain. The appearance of non-Gaussian noise components at lower temperatures can be seen as an indication of freezing of the electronic system into the Coulomb glass state [4,7,36,37].

RTN switching rate is thermally activated, meaning that the system has to overcome a certain energy barrier in order to switch between RTN states. Permanence of the system in *up* or *down* RTN states is associated with current percolating through local clusters constituted by different phases with different resistivity which may be characterized by substantially different energies and entropies. The schematic of the energy structure of the TLF is shown in the inset to Fig. 13. The average lifetimes of the *up* and *down* state τ_{up} and τ_{dn}, respectively, can be written as

$$\tau_{up} = \tau_{0up} \exp\left[(F_0 + \Delta F/2)/k_B T\right],$$
$$\tau_{dn} = \tau_{0dn} \exp\left[(F_0 - \Delta F/2)/k_B T\right], \quad (4)$$

where τ_{0up} and τ_{0dn} are prefactors related to the frequency of phonos, k_B is the Boltzmann constant, and T is the temperature. Assuming that $\tau_{0up} = \tau_{0dn} = \tau_0$, the free energy difference ΔF between RTN *up* and *down* states can now be written in terms of the ratio between the average lifetimes of the *up* and *down* states $r = \tau_{up}/\tau_{dn}$ as $\Delta F = k_B T \ln r$. Thus the determined free energy difference between the RTN states is shown as a function of temperature in Fig. 13. Observe that ΔF increases almost linearly with increasing temperature up to $T \approx T_c$, while in the nominally PM regime, $T > T_c$, ΔF is practically temperature independent.

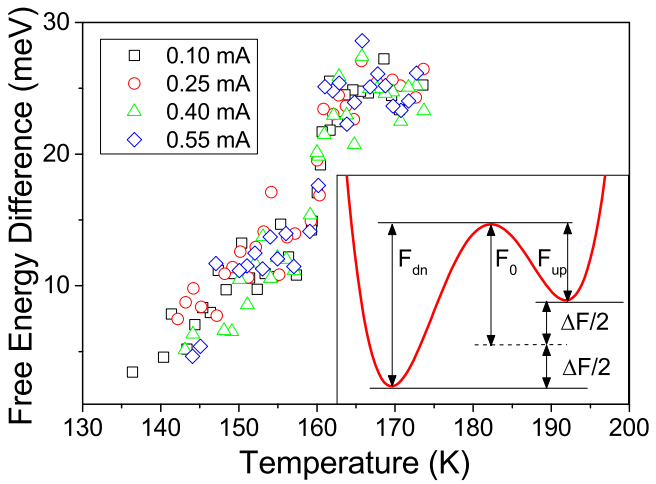

FIG. 13. Free energy difference between RTN states. Inset shows a free energy model of a TLF.

V. CONCLUSIONS

Conductivity of $La_{0.86}Ca_{0.14}MnO_3$ single crystals in the low-resistivity state exhibits random telegraph fluctuations of unusual properties. Namely, telegraph fluctuations appear only in the low-resistivity state and vanish upon sample transition to the high-resistivity state. The thermally activated two-level fluctuator persists and can be continuously followed in exceptionally wide temperature range of the order of 50 K. The thermally activated switching rate of the fluctuator is completely independent of the applied bias current and magnetic field. The amplitude of the telegraph signal depends nonmonotonically on temperature and decreases exponentially with increasing bias current.

Analysis of the features of the telegraphic conductivity fluctuations combined with comprehensive structural, transport, magnetic, and resonant properties of the investigated crystals indicate that dynamic current redistribution mechanism is responsible for the observed noise and explains the peculiar features of the telegraph conductivity fluctuations. The essential ingredients of the proposed mechanism are the phase separation, enabling coexistence of percolating paths with different resistivity, and a positive feedback mechanism coming from a positive derivative of the sample resistivity $\rho(T,I)$ versus bias current $\partial\rho(T,I)/\partial I > 0$.

As revealed by the resonance measurements, already at 240 K, above the Curie temperature, clusters of ferromagnetic metallic phase FM1 start to coexist with a paramagnetic insulating matrix. The density of ferromagnetic clusters increases with decreasing temperature and around 185 K it allows for formation of lower resistivity percolation paths in the paramagnetic matrix. Below the main paramagnetic to ferromagnetic transition, the role of the insulating matrix is played by the dominant ferromagnetic insulating phase FM2, occupying about 90% of the sample volume.

The mechanism responsible for robust random telegraph conductivity fluctuations appearing in very wide temperature range is dynamic current redistribution consisting in thermally activated switching between different current flow patterns and current-dependent resistivity of the discussed system. The telegraph signal ceases to exist when decreasing temperature approaches T_R at which the resistivity becomes current independent.

The absence of telegraph fluctuations in the high-resistivity state can be also understood in the framework of the proposed dynamic current redistribution mechanism. Observe that resistivity of HRS is markedly less influenced by the current flow than that of LRS; see Fig. 3. Therefore, the feedback factor $R_h(T) - R(I,T)$ is too small to allow for the appearance of RTN fluctuations with measurable amplitude.

For a full understanding of the physics involved in the telegraph conductivity fluctuations, one needs to explain the conductivity mechanisms leading to particular current dependence of the resistivity and the feedback effect. These issues are subjects of our ongoing investigations.

ACKNOWLEDGMENT

This work was supported by the Polish National Science Centre (NCN) Grant No. 2012/05/B/ST3/03157.

[1] G. Papavassiliou, M. Pissas, M. Belesi, M. Fardis, J. Dolinsek, C. Dimitropoulos, and J. P. Ansermet, Phys. Rev. Lett. **91**, 147205 (2003).
[2] M. Pissas and G. Papavassiliou, J. Phys.: Condens. Matter **16**, 6527 (2004).
[3] M. Pissas, G. Papavassiliou, E. Devlin, A. Simopoulos, and V. Likodimos, Eur. Phys. J. B **47**, 221 (2005).
[4] S. Samanta, A. K. Raychaudhuri, and Ya. M. Mukhovskii, Phys. Rev. B **85**, 045127 (2012).
[5] P. A. Kumar, R. Mathieu, P. Nordblad, S. Ray, O. Karis, G. Andersson, and D. D. Sarma, Phys. Rev. X **4**, 011037 (2014).
[6] E. Bose, S. Karmakar, B. K. Chaudhuri, and S. Pal, Sol. State Commun. **145**, 149 (2008).
[7] A. Amir, Y. Oreg, and Y. Imry, Ann. Phys. **18**, 836 (2009).
[8] Y. Yuzhelevski, V. Markovich, V. Dikovsky, E. Rozenberg, G. Gorodetsky, G. Jung, D. A. Shulyatev, and Y. M. Mukovskii, Phys. Rev. B **64**, 224428 (2001).
[9] V. Markovich, G. Jung, Y. Yuzhelevski, G. Gorodetsky, A. Szewczyk, M. Gutowska, D. A. Shulyatev, and Ya. M. Mukovskii, Phys. Rev. B **70**, 064414 (2004).
[10] V. Markovich, G. Jung, Y. Yuzhelevskii, G. Gorodetsky, F. X. Hu, and J. Gao, Phys. Rev. B **75**, 104419 (2007).
[11] X. D. Wu, B. Dolgin, G. Jung, V. Markovich, Y. Yuzhelevski, M. Belogolovskii, and Ya. M. Mukovskii, Appl. Phys. Lett. **90**, 242110 (2007).
[12] B. Dolgin, M. Belogolovskii, X. D. Wu, V. Markovich, and G. Jung, J. Appl. Phys. **112**, 113907 (2012).
[13] A. Anane, B. Raquet, S. von Molnar, L. Pinsard-Godart, and A. Revcolevschi, J. Appl. Phys. **87**, 5025 (2000).
[14] H. T. Hardner, M. B. Weissman, M. Jaime, R. E. Treece, P. C. Dorsey, J. S. Horwitz, and D. B. Chrisey, J. Appl. Phys. **81**, 272 (1997).
[15] R. D. Merithew, M. B. Weissman, F. M. Hess, P. Spradling, E. R. Nowak, J. O'Donnell, J. N. Eckstein, Y. Tokura, and Y. Tomioka, Phys. Rev. Lett. **84**, 3442 (2000).
[16] B. Raquet, A. Anane, S. Wirth, P. Xiong, and S. von Molnar, Phys. Rev. Lett. **84**, 4485 (2000).
[17] A. Palanisami, R. D. Merithew, M. B. Weissman, and J. N. Eckstein, Phys. Rev. B **64**, 132406 (2001).
[18] A. Asamitsu, Y. Tomioka, H. Kuwahara, and Y. Tokura, Nature (London) **388**, 50 (1997).
[19] S. Wirth, A. Anane, B. Raquet, and S. von Molnar, J. Magn. Magn. Mater. **290-291**, 1168 (2005).
[20] Y. Yuzhelevski, V. Dikovsky, V. Markovich, G. Gorodetsky, G. Jung, D. A. Shulyatev and Ya. M. Mukovskii, Fluct. Noise Lett. **01**, L105 (2001).
[21] A. Bid, A. Guha, and A. K. Raychaudhuri, Phys. Rev. B **67**, 174415 (2003).
[22] T. Z. Ward, X. G. Zhang, L. F. Yin, X. Q. Zhang, Ming Liu, P. C. Snijders, S. Jesse, E. W. Plummer, Z. H. Cheng, E. Dagotto, and J. Shen, Phys. Rev. Lett. **102**, 087201 (2009).
[23] J. Przybytek, J. Fink Finowicki, R. Puźniak, V. Markovich, and G. Jung, J. Appl. Phys. **118**, 043903 (2015).
[24] A. I. Shames, E. Rozenberg, G. Gorodetsky, and Ya. M. Mukovskii, Phys. Rev. B **68**, 174402 (2003).
[25] V. Likodimos and M. Pissas, Phys. Rev. B **73**, 214417 (2006).
[26] E. Rozenberg, A. I. Shames, M. Auslender, G. Jung, I. Felner, J. Sinha, S. S. Banerjee, D. Mogilyansky, E. Sominski, A. Gedanken, Ya. M. Mukovskii, and G. Gorodetsky, Phys. Rev. B **76**, 214429 (2007).
[27] J. A. Mydosh, *Spin Glasses* (Taylor and Francis, London, 1993).
[28] J. Wu and C. Leighton, Phys. Rev. B **67**, 174408 (2003).
[29] A. I. Shames and E. Rozenberg, J. Phys.: Condens. Matter **20**, 058001 (2008).
[30] V. A. Atsarkin and V. V. Demidov, J. Exp. Theor. Phys. **103**, 589 (2006).
[31] V. N. Krivoruchko, Low Temp. Phys. **40**, 586 (2014).
[32] E. Rozenberg, M. Auslender, A. I. Shames, I. Felner, D. Mogilyansky, and Ya. M. Mukovskii, J. Appl. Phys. **109**, 07D902 (2011); E. Rozenberg, J. Alloys Compd. **602**, 40 (2014).
[33] C. Barone, S. Pagano, L. Méchin, J.-M. Routoure, P. Orgiani, and L. Maritato, Rev. Sci. Instrum. **79**, 053908 (2008).
[34] M. B. Weissman, Rev. Mod. Phys. **65**, 829 (1993).
[35] G. T. Seidler, S. A. Solin, and A. C. Marley, Phys. Rev. Lett. **76**, 3049 (1996).
[36] A. Sahoo, S. D. Ha, S. Ramanathan, and A. Ghosh, Phys. Rev. B **90**, 085116 (2014).
[37] V. Orlyanchik, M. B. Weissman, M. A. Torija, M. Sharma, and C. Leighton, Phys. Rev. B **78**, 094430 (2008).